Sensitivity of observables to coarse-graining size in heavy-ion collisions

Fernando G. Gardim,[1] Frédérique Grassi,[2] Pedro Ishida,[2] Matthew Luzum,[2] Pablo S. Magalhães,[1] and Jacquelyn Noronha-Hostler[3]

[1]*Instituto de Ciência e Tecnologia, Universidade Federal de Alfenas, 37715-400 Poços de Caldas-MG, Brazil*

[2]*Instituto de Física, Universidade de São Paulo, Rua do Matão 1371, 05508-090 São Paulo-SP, Brazil*

[3]*Department of Physics and Astronomy, Rutgers, The State University of New Jersey, Piscataway, New Jersey 08854-8019, USA*

(Received 15 February 2018; published 29 June 2018)

An open question in the field of heavy-ion collisions is to what extent the size of initial inhomogeneities in the system affects measured observables. Here we present a method to smooth out these inhomogeneities with minimal effect on global properties, to quantify the effect of short-range features of the initial state. We show a comparison of hydrodynamic predictions with original and smoothened initial conditions for four models of initial conditions and various observables. Integrated observables (integrated v_n, scaled v_n distributions, normalized symmetric cumulants, event-plane correlations) as well as most differential observables [$v_n(p_T)$] show little dependence on the inhomogeneity sizes and instead are sensitive only to the largest-scale geometric structure. However, other differential observables such as the flow factorization ratio and subleading principal components are more sensitive to the granularity and could be a good tool to probe the short-scale dynamics of the initial stages of a heavy-ion collision, which are not currently well understood.

DOI: 10.1103/PhysRevC.97.064919

I. INTRODUCTION

Relativistic heavy-ion collisions are being performed at RHIC and the LHC to study the quark gluon plasma. The aim is to extract its transport properties, phase diagram, and initial state. Understanding its initial state, for instance, can help clarify details of strong interactions away from equilibrium. In the standard picture of a relativistic heavy-ion collision, the system rapidly thermalizes and expands hydrodynamically (for recent reviews, see Refs. [1–4]). Ultimately, the system decouples and particles are emitted. However, the initial stages of the collisions, before the system has sufficiently thermalized to exhibit hydrodynamic behavior, are still poorly understood. Hydrodynamic simulations therefore rely on models to provide initial conditions, of which many exist, with various features and levels of sophistication. There are differences in the source of fluctuations in each of these different initial condition models, for instance, contributions of the quarks and gluons to fluctuations versus assuming only nucleonic fluctuations, which translates into different scales of structure.

In models based on the Monte Carlo Glauber model [5–7], nucleons follow straight-line trajectories and make collisions. In coordinate space the positions of the wounded nucleons are like δ function, thus, two-dimensional Gaussians are used to smear the colliding nucleons. The usual source of fluctuations is the position of the nucleons so the size of the hot spots reflects roughly the radius of a proton ($\sim$1 fm). More recently an alternative to the standard wounded nucleon picture was created using parameterized version of initial conditions, TRENTO [8]. At this point in time, subnucleonic degrees of freedom have not yet been included in the public version.

More sophisticated models with nontrivial dynamics are also employed such as NeXus [9], EPOS [10], UrQMD [11,12], and AMPT [13]. These can involve various scales: In the NeXus model [9], parton ladders are exchanged between nucleons, fluctuations occur both at the nucleonic level—nucleon positions fluctuate—and partonic level—energy sharing to produce the ladders is probabilistic but the hot spot size also reflects the nucleon size [14]. This is illustrated in the first row of Fig. 1.

Models based on perturbative QCD combined with saturation physics also exist, such as the EKRT model [15]. Finally, there are models based on the color-glass-condensate effective theory, most notably MC-KLN [16] and IP-Glasma [17]. In the MC-KLN model [16], at a certain point in the transverse plane (x, y) the energy density depends on the saturation scale, which is related to the nuclear thickness functions through the k_t-factorization formula. Nucleonic fluctuations are considered in mckln, although small uncorrelated hot spots appear in certain versions, as shown in the bottom row of Fig. 1. In the IP-Glasma model [17], fluctuations of nucleon positions as well as subnucleonic fluctuations of color charges are included. The resulting hot spot size is significantly smaller [17] than other models.

Many of these models have been quite successful in reproducing experimental data (for a few recent comparisons, see Refs. [18–23]). However, each of these models has differences in the macroscale—i.e., the shape and size of the initial conditions, the size and location of the hot spots, and the strength of the fluctuations, such that it is not always clear exactly which features are essential for reproducing a given observable. In particular, many observables can be simultaneously reproduced by different initial condition models, providing the transport properties and other relevant parameters are properly adjusted. Significant work has been done in terms of constraining the degree of fluctuations in initial conditions

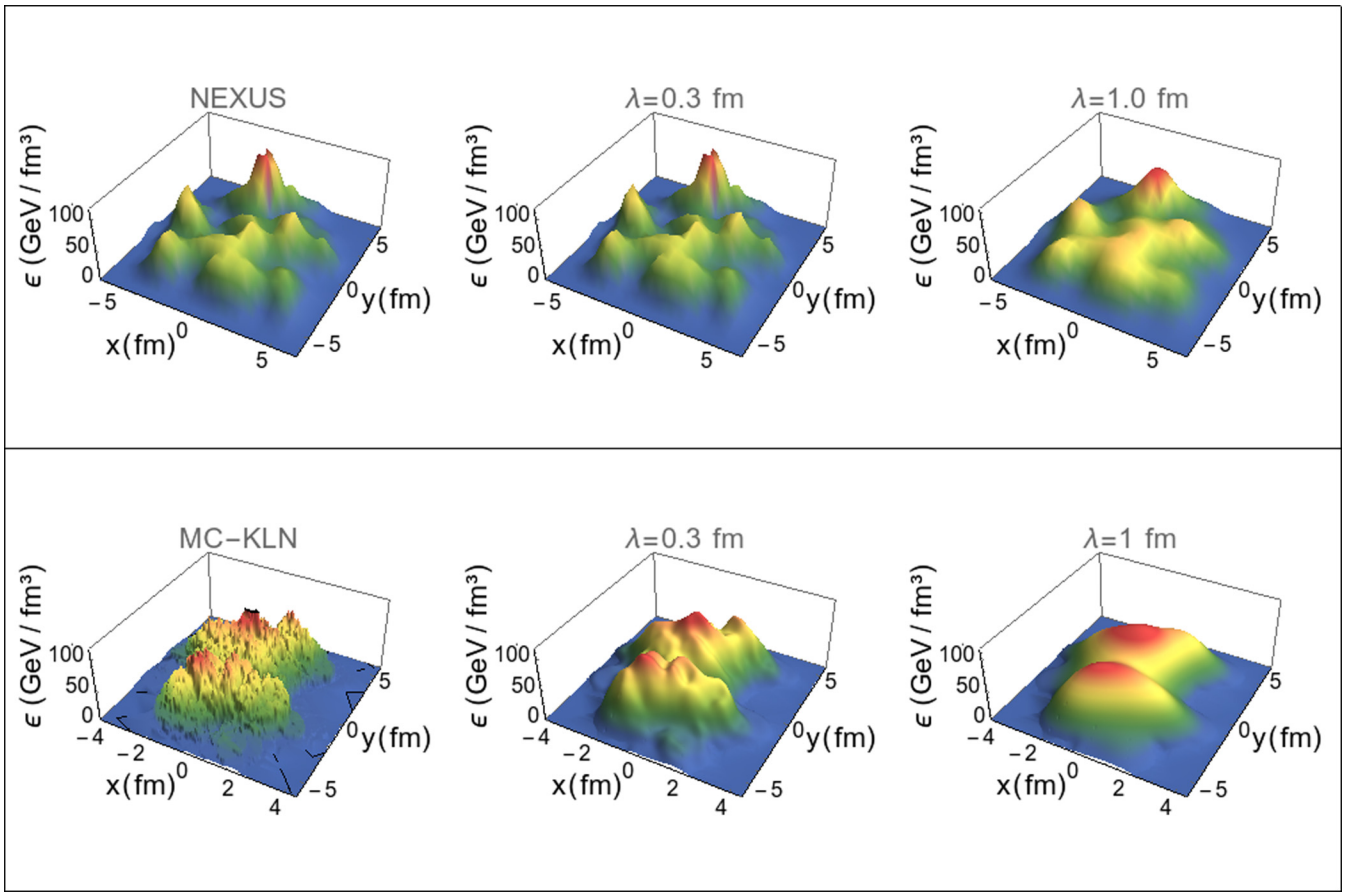

FIG. 1. Top: NeXus initial energy density in a midrapidity transverse plane without modification and modified by a cubic spline filter with $\lambda = 0.3$ and 1 fm. This corresponds to a central Pb-Pb collision at $\sqrt{s_{\rm NN}} = 2.76$ TeV. Bottom: MC-KLN initial energy density in a midrapidity transverse plane without modification and modified by a cubic spline filter with $\lambda = 0.3$ and 1 fm. This corresponds to a noncentral Pb-Pb collision at $\sqrt{s_{\rm NN}} = 2.76$ TeV.

using multiparticle cumulants [21] and event-by-event flow distributions [24].

One open question is whether the spatial extent of "hot spots" in the initial system—which can be quite different in different models—has a sizable effect on measured observables. This is an important question if we want to rule out models for the initial state and elucidate the dynamics of the strong interactions. Typically this is studied by smoothening small-scale inhomogeneities in a particular model for the initial state and comparing final observables to the unaltered version. In this way, one can compare initial conditions that have the same large-scale structure, but differ only at small length scales, and therefore detect any dependence of measured observables on small-scale features of the initial state.

Most commonly a Gaussian function is used to smooth out small-scale fluctuations [24–33]. However, this procedure not only smoothens small-scale inhomogeneities, but simultaneously increases the radius of the system. This changes the global structure, making the initial conditions rounder [34], and therefore makes it more difficult to discern a small dependence on small structures from a well-understood dependence on global eccentricities. More recently, cubic splines have been used [35], which smooth out fluctuations to a finite radius, thus, preserving the initial eccentricities to larger smoothing scales [35].

It should be noted that the idea is not to study specific dynamical processes that might naturally make the system smoother [36], but instead to search for observables that might be used to probe physics at small scales.

The objective of this paper is therefore the following: we consider four initial state models and smooth the size of their inhomogeneities on scale from 0.3 to 1 fm (we do not go further since this is the typical range of nucleonic inhomogeneities). We then compare predictions for observables for the original model and its smoothed versions. We find that the differences are in fact very small for a large range of observables: integrated v_n, scaled v_n distributions, normalized symmetric cumulants, event plane correlations, and $v_n(p_T)$. We observe larger differences for the flow factorization ratios r_n and the subleading modes in a principal component analysis of the two-particle correlation matrix, which are therefore the most promising observables for probing scales smaller than the system size.

The outline of this paper is as follows. In Sec. II, we recall how to characterize the initial and final states through eccentricities and harmonic flow coefficients. In Sec. III, we describe our smoothing method. In Sec. IV, we present our results for integrated and p_T dependent quantities. Finally in Sec. V, we discuss our findings.

II. CHARACTERIZING THE INITIAL AND FINAL STATES

The initial conditions for hydrodynamic evolution consist of the energy-momentum tensor at some initial time $T^{\mu\nu}(\tau = \tau_0)$. It is believed that the most important aspect of the initial conditions for observables near midrapidity is the energy density in the transverse plane $\epsilon(x,y) = T^{\tau\tau}(\tau_0, \eta \sim 0, x, y)$. Hydrodynamic evolution converts this geometry into the final momentum distribution of detected particles.

We would like to characterize this initial density distribution in a way that is ordered according to length scale. The natural way to do this is to switch to Fourier transformed coordinates, such that small k represents large-scale structure and large k represents small-scale structure.

Specifically, we define the transformed density via a 2D Fourier transform [37],

$$\rho(\vec{k}) = \int d^2x \epsilon(\vec{x}) e^{-i\vec{k}\cdot\vec{x}}, \tag{1}$$

from which we create a cumulant generating function,

$$e^{W(\vec{k})} \equiv \rho(\vec{k}), \tag{2}$$

that we expand in a power series around $k \equiv |\vec{k}| = 0$:

$$W(\vec{k}) = \sum_{m=0}^{\infty} W_m(\phi_k) k^m. \tag{3}$$

It is useful to encode the dependence on azimuthal angle ϕ_k in a Fourier series, to obtain a discrete set of coefficients that contain all information about the distribution of energy density $\epsilon(x,y)$,

$$W(\vec{k}) = \sum_{m=0}^{\infty} \sum_{n=-\infty}^{\infty} W_{n,m} k^m e^{-in\phi_k}. \tag{4}$$

The coefficients with smallest m, therefore, represent information about the largest-scale, global structure, while larger m represents smaller-scale structures in the initial geometry. The value of n represents the rotational property of each coefficient.

Note that nonzero coefficients must have $m \geqslant n$, and $m - n$ must be even. So for a given Fourier harmonic n, the lowest cumulant is $W_{n,n}$.

This expression can be inverted to obtain explicit equations for the coefficients $W_{n,m}$ (called cumulants, since they have the same relation to the distribution of energy as traditional cumulants have to a probability distribution). We list a few of the lowest cumulants here, defining the complex coordinate $z \equiv x + iy$:

$$W_{0,0} = \ln E, \tag{5}$$

$$W_{1,1} \propto \langle z \rangle, \tag{6}$$

$$W_{0,2} \propto \langle |z|^2 \rangle, -\langle z \rangle \langle \bar{z} \rangle, \tag{7}$$

$$W_{2,2} \propto \langle z^2 \rangle - \langle z \rangle^2, \tag{8}$$

$$W_{1,3} \propto \langle z^2 \bar{z} \rangle - \langle z^2 \rangle \langle \bar{z} \rangle - 2\langle |z|^2 \rangle \langle z \rangle + 2\langle z \rangle^2 \langle \bar{z} \rangle,$$

$$W_{3,3} \propto \langle z^3 \rangle + \langle z \rangle (3\langle z^2 \rangle - 2\langle z \rangle^2), \tag{9}$$

with

$$\langle \ldots \rangle = \frac{\int d^2x \epsilon(\mathbf{x}) \ldots}{\int d^2x \epsilon(\mathbf{x})}, \tag{10}$$

and E is the total energy $E = \int d^2x \epsilon(\mathbf{x})$.

With this construction, all cumulants are invariant under translations, except $W_{1,1}$, which represents the center of the system. They are therefore appropriate for making a connection to the final momentum-space particle distributions, which do not depend on the choice of coordinate center.

To study dimensionless observables such as anisotropic flow, it is useful to define dimensionless ratios out of the lowest cumulants for each azimuthal harmonic n, whose magnitude and phase are the standard eccentricities ε_n and participant planes Φ_n:

$$\mathcal{E}_2 = \varepsilon_2 e^{2i\Phi_n} \equiv -2\frac{W_{2,2}}{W_{0,2}} = -\frac{\langle z^2 \rangle}{\langle |z|^2 \rangle} = -\frac{\langle r^2 e^{2i\phi} \rangle}{\langle r^2 \rangle}, \tag{11}$$

$$\mathcal{E}_3 \equiv -\frac{\langle r^3 e^{3i\phi} \rangle}{\langle r^3 \rangle}, \tag{12}$$

$$\mathcal{E}_1 \equiv -\frac{\langle r^3 e^{i\phi} \rangle}{\langle r^3 \rangle}, \tag{13}$$

etc., where it is understood that the center of coordinates is chosen in each event such that $W_{1,1} = 0$, which significantly simplifies the expressions.

If we also expand the final single-particle momentum distribution in an azimuthal Fourier series,

$$\frac{dN}{d\phi_p} = \frac{N}{2\pi} \sum_n V_n e^{-in\phi_p}, \tag{14}$$

with

$$V_n \equiv v_n e^{in\Psi_n} = \frac{1}{N} \int d\phi_p e^{in\phi_p} \frac{dN}{d\phi_p}, \tag{15}$$

(Differential $V_n(p_T, \eta)$ can be defined in a similar way.)

We can conjecture event-by-event vector relations such as

$$V_2 \propto \mathcal{E}_2,$$
$$V_3 \propto \mathcal{E}_3. \tag{16}$$

It has been shown that these relations are quite accurate, on an event-by-event basis [15,38,39] and for differential measurements as well [40–42].

This is a very deep statement about the nature of hydrodynamic behavior—the eccentricities ε_n represent only the lowest in an infinite series of cumulants with harmonic n, representing global properties at the largest length scales. Even in cases where a nonlinear dependence on eccentricities is known (such as v_4 and v_5 in noncentral collisions), the fact that it depends only on eccentricities $\mathcal{E}_n$ still indicates that the final observables are dominated by structures in the initial energy density at the longest length scales.

It is therefore known that momentum integrated, as well as differential, flow depends mostly on the largest length scales, as represented by eccentricities ε_n. However, the above relations are not 100% precise, and there is room for some sensitivity to structures in the initial state at smaller length scales.

In this work, we investigate this possible sensitivity to the granularity of the initial energy density profile in the transverse plane and want to find observables that can best probe these features. To do this, we must establish a dependence of these observables on higher cumulants $W_{n,m}$, with $m > n$, beyond any dependence on eccentricities, which only represent global properties.

III. SMOOTHING METHOD

To investigate the influence of coarse-graining sizes on observables, we modify the initial conditions for each event using a filter. The aim is to smooth the energy density profile, such that global properties (as represented by eccentricities ε_n) are kept relatively unchanged, but small-scale structure (quantified by higher cumulants with $m > n$) is different. This allows us to investigate the dependence on the granularity of the initial state.

The filter we use is based on cubic splines and was described (for the two-dimensional case) in Ref. [35]. For completeness we reproduce part of the discussion here. The idea is that the transverse energy density value at some point is determined as a weighted sum of energy density values at fixed points $\vec{r}_\alpha$ around it in the transverse plane, with nearest points contributing more.

$$\epsilon(\tau_0,\vec{r};\lambda) = \sum_{\alpha=1}^{N} \epsilon(\tau_0,\vec{r}_\alpha) W\left(\frac{|\vec{r}-\vec{r}_\alpha|}{\lambda};\lambda\right), \tag{17}$$

where W is given by

$$W\left(\frac{|\vec{r}|}{\lambda};\lambda\right) = \frac{10}{7\pi\lambda^2} f\left(\frac{|\vec{r}|}{\lambda}\right) \tag{18}$$

and

$$f(\xi) = \begin{cases} 1 - \frac{3}{2}\xi^2 + \frac{3}{4}\xi^3 & \text{if } 0 \leqslant \xi < 1 \\ \frac{1}{4}(2-\xi)^3 & \text{if } 1 \leqslant \xi \leqslant 2, \\ 0 & \text{if } \xi > 2 \end{cases} \tag{19}$$

where α is the index of the points used for the approximation, and N is their total number. As shown by Eq. (19), only approximation points within 2λ of the point at $\vec{r}$ contribute to its energy density. We use values $\tau_0 = 1$ fm and 0.6 fm, respectively, for the codes NeXSPheRIO and v-USPhydro (described in the next section). We note that W is peaked at $\vec{r} = 0$, nonnegative, invariant under parity and satisfies $\int W(\frac{|\vec{r}|}{\lambda};\lambda)d\vec{r} = 1$ so the integral of $\epsilon(\tau_0,\vec{r};\lambda)$ on the transverse plane is not modified by a change in λ.

This procedure preserves the total energy of the system, but can alter the entropy due to the nonlinear relationship between the two quantities. However, we have checked that the entropy of individual events is not substantially changed: for NeXus initial conditions, the largest relative change was never more than 4%.

The advantage of this filter is that it has a compact support and we have a good control of its effect when changing the value of the parameter λ.

Figure 1 shows the effect of the filters on a typical event generated with NeXus. The cubic spline filter with $\lambda = 1$ fm maintains the locations of the main pikes and valleys but smooth them so that their spatial extent increases. The cubic spline filter with $\lambda = 0.3$ fm has little effect as expected since the relevant scale for NeXus initial conditions is the nucleon size. The effect of the cubic spline filter is also illustrated for MC-KLN. Since the initial inhomogeneities occur on a smaller scale, the effect of the filter is stronger for small values of λ.

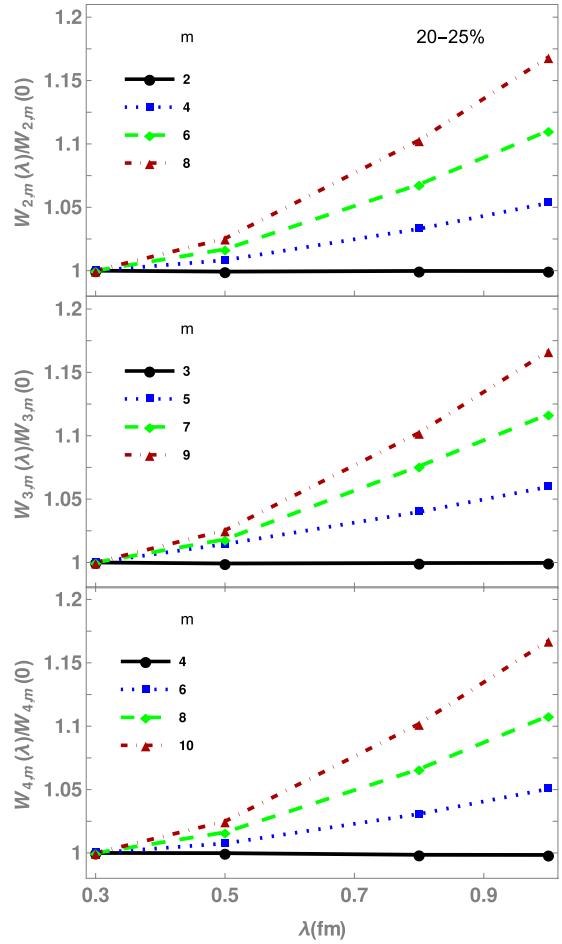

FIG. 2. Cumulants $W_{n,m}$ as a function of smoothing parameter λ for NeXus events in the 20–25% centrality bin. Each cumulant is normalized by its value without smoothing $W_{n,m}(0)$.

In Fig. 2, we show the effect of the smoothing on cumulants $W_{n,m}$ for a set of NeXus events in the 20–25% centrality bin. We can see the lowest anisotropic cumulants $W_{n,n}$ are essentially unaffected by smoothing, while higher cumulants depend on the value of the smoothing parameter λ, with increasing sensitivity for cumulants of larger m, as expected.

Note, however, that the smoothing process does have a small effect on $n = 0$ cumulants—i.e., the size of the system—as shown in the bottom plot of Fig. 3. The average radius of the system increases by ∼2.5% when the smoothing parameter is changed from 0 to 1 fm, or $\langle r^n\rangle \to 1.025^n\langle r^n\rangle$. The corresponding eccentricities therefore *decrease* by roughly $n \times 2.5\%$. This is illustrated in the top plot of Fig. 3.

Any effect that can be explained by this decrease is therefore *not* a dependence on initial state granularity but only on the well-known dependence on large-scale structure. For example, if a quantity scales with eccentricity, only changes by more than n times the relevant factor are indicative of a dependence on

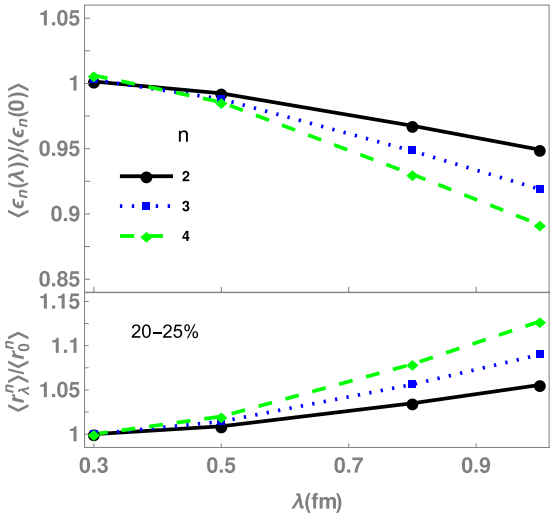

FIG. 3. Top: $\langle\epsilon_n\rangle$ as a function of smoothing parameter λ for NeXus events in the 20–25% centrality bin. Each $\langle\epsilon_n\rangle$ is normalized by its value without smoothing $\langle\epsilon_n(0)\rangle$. Bottom: Similar plots for $\langle r^n\rangle$.

small scale. If a ratio of two quantities scaling with eccentricity is considered, any change (greater than statistical uncertainty) can be indicative of a dependence on small scale.

Because of this, it is important to use a smoothing procedure that does not significantly increase the size of the system, and this is why in this work we use a filter with compact support.

For MC-KLN, a similar decrease of eccentricities with λ is observed [35].

IV. RESULTS FOR OBSERVABLES

In this paper, we perform simulations with two codes. Both use the smoothed particle hydrodynamics Lagrangian algorithm developed in Ref. [43].

NeXSPheRIO (the first event-by-event code developed for relativistic heavy-ion collisions) solves the perfect fluid hydrodynamic equations in 3+1 dimensions. The initial conditions are obtained event-by-event with the NeXus generator [9]. The equation of state matches lattice data at zero baryonic potential and has a critical point added in a phenomenological way [44]. Isothermal Cooper-Frye freeze-out is used with temperatures chosen in each centrality window to match observables. At top RHIC energies, this code has successfully reproduced a number of data [45–52]. An extension to LHC energies ($\sqrt{s_{\rm NN}} = 2.76$ TeV Pb+Pb collisions) was developed in Ref. [53] and is used here. The code was tested against known solutions in Ref. [43]. There is a 2+1 version of NeXSPheRIO with longitudinal boost invariance that is used here to facilate comparison with the second code described below.

This second code, v-USPhydro [54,55], solves viscous fluid hydrodynamic equations in 2+1 dimensions assuming longitudinal boost invariance. Here it is used to calculate the flow harmonics from MC-KLN initial conditions (for $\sqrt{s_{\rm NN}} =$ 2.76 TeV Pb+Pb collisions). Both (temperature dependent) bulk and shear viscosities can be considered [54,55]. For simplicity's sake, only constant shear viscosity is assumed and adjusted to obtain a reasonable description of LHC data. The lattice-based equation of state S95n-v1 from [56] and an isothermal Cooper-Frye freezeout are used (although this choice may affect η/s at high energies [20]). v-USPhydro was shown to reproduce TECHQM test [57] as well as both the analytical and semi-analytical radially expanding solutions of Israel-Stewart hydrodynamics [58].

Note that in the following we also show results from smoothing out IP-Glasma and MC-Glauber initial conditions but do not run them through hydrodynamics.

A. Integrated observables

As we have seen in Fig. 3, the eccentricities are little affected by the smoothing length for NeXus initial conditions, changing at most by $n \times 2.5\%$. Due to the strong event-by-event correlation between final flow and initial eccentricity Eq. (16), we expect a similar change in integrated flow observables.

To test this, in Fig. 4 we show the ratio $\langle v_n\rangle/\langle\varepsilon_n\rangle$ using different smoothing lengths. Most of the change in integrated v_n is compensated by the change in ε_n, with only a slight residual dependence, in particular for v_4, which is known to not follow eccentricity scaling. There is no indication of a significant dependence on small-scale structure, and instead the results are determined by the global structure of the initial conditions.

We can make even more precise tests by considering scaled observables that are approximately independent of the small change in system size from our smoothing procedure.

Therefore, we next consider event-by-event distributions of anisotropic flow $P(v_n)$ [59–61]. Equation (16) suggests that a uniform change in eccentricity should result in a uniform change in the distribution of v_n. If we divide the distribution by the mean, the result $P(v_n/\langle v_n\rangle)$ should then be independent of such a rescaling of eccentricity.

This is the reason, for example, that scaled distributions of flow coefficients depend little on viscosity, and instead directly probe the initial conditions [15,38]. Because of this, one can immediately see that some models are incompatible with measured data [59,60], while others [15,62,63] agree with data (the latter includes the NeXus model used in this work [64]).

To study the effect of smoothing, we first consider the $P(\epsilon_n/\langle\epsilon_n\rangle)$ distributions. Results for NeXus initial conditions and ideal hydrodynamics are shown for the 20–25% centrality window in Fig. 5. No dependence on the value of λ is seen,

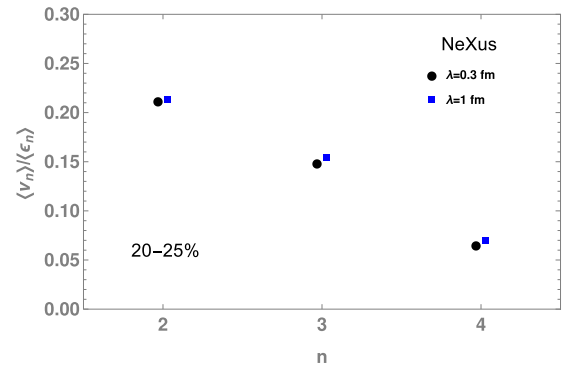

FIG. 4. Comparison of original and filtered eccentricity scaled flow harmonics $\langle v_n\rangle/\langle\varepsilon_n\rangle$ for the 20–25% centrality window.

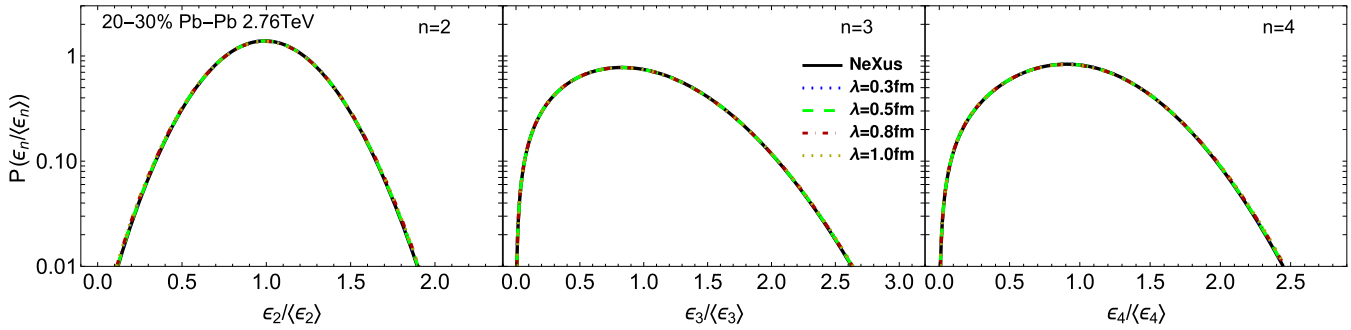

FIG. 5. Comparison of original and filtered scaled ϵ_n probability distributions for NeXus initial condition in the 20–30% windows.

indicating that smoothing essentially corresponds to a uniform rescaling of ε_n (in turn caused by a uniform scaling of the system size $\langle r^n \rangle$).

One might think that these small differences are due to the fact that in NeXus the typical inhomogeneities have nucleonic size, which is comparable to the maximum λ considered. More striking results are shown in Fig. 6. The original and filtered ($\lambda = 1$ fm) eccentricity distributions for IP-Glasma [17], MC-KLN [16], and MC-Glauber [5–7] models were obtained for the 20–30% centrality window. One sees that for these models, the scaled eccentricity distributions are insensitive to the smoothing length below 1 fm. Similar results hold for other centralities.

However deviation from Eq. (16) are known to happen; e.g., elliptic flow v_2 does not grow perfectly linearly with ϵ_2 for noncentral collisions [15,38,39,65].

Therefore it is important to compute v_n distributions, to determine whether the small deviation from linearity is due to higher cumulants and small-scale structure, or simply a nonlinear dependence on eccentricities, so that only global properties are important. The most interesting case is a noncentral bin for $n = 2$ since it was observed [24,60] that v_2 distributions for central collisions as well as v_3 and v_4 distributions for all centralities do not depend on the details of the initial conditions. The scaled v_2 distributions for the original and filtered initial conditions are compared for MC-KLN in Fig. 7 for the 20–30% centrality window. They too are independent of the value of λ.

We conclude that integrated flow $v_n\{2\}$ and event-by-event distributions of anisotropic flow coefficients have little dependence on the smoothing length for the four models considered in this paper, and instead depend only on global features of the initial conditions. To continue our search for variables that depend on the coarse-graining size, we note that v_n distributions contain information only about a single Fourier harmonic n. It is then interesting to study mixed harmonic observables, in particular those that are experimentally measurable [66,67] or may be obtained at RHIC [68].

We consider normalized symmetric cumulants:

$$\mathrm{NSC}(n,m) = \frac{\langle v_n^2 v_m^2 \rangle - \langle v_n^2 \rangle \langle v_m^2 \rangle}{\langle v_n^2 \rangle \langle v_m^2 \rangle}. \tag{20}$$

We note that the connection between these quantities and their equivalent ones computed with eccentricities is not one-to-one. In Ref. [69], it was argued that NSC(2,3) and NSC(3,4) depend little on the initial conditions while NSC(2,4) does. In Fig. 8, one can see that the precise coarse-graining size does not matter even for NSC(2,4) for NeXus and MC-KLN initial conditions.

We can go a step further and consider event plane correlations which mix both magnitude and event planes and have been measured by ATLAS [70]. However, we also found no dependence on the smoothing length for these observables.

B. Differential observables

From $\lambda = 0.3$–1 fm no clear evidence of a sensitivity to coarse-graining could be found in p_T integrated observables of all charged particles. Additional information can be obtained from differential quantities, which we now consider. Transverse momentum spectra for different coarse-graining sizes

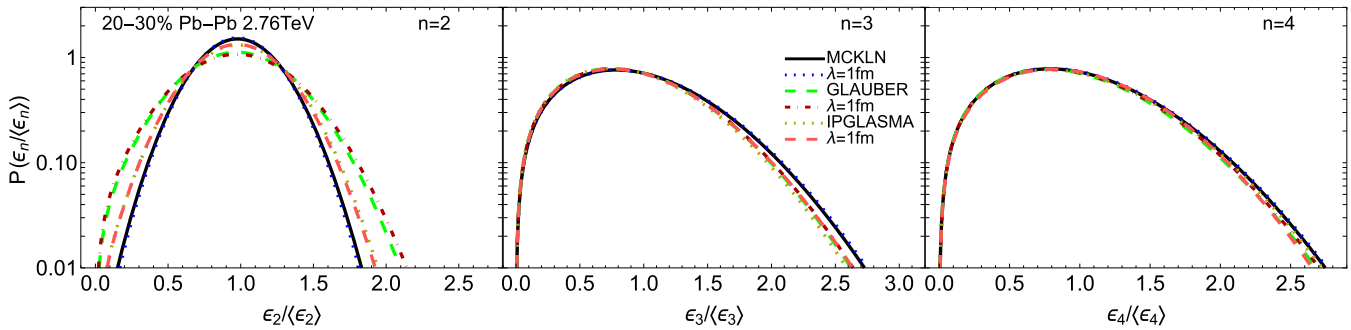

FIG. 6. Comparison of original and filtered scaled ϵ_n probability distributions for various models of initial conditions in the 20–30% windows. In the legend, lines 1, 3, and 6 indicate the symbols for the original initial conditions and lines 2, 4, and 6 for their respective filtered $\lambda = 1\ fm$ versions.

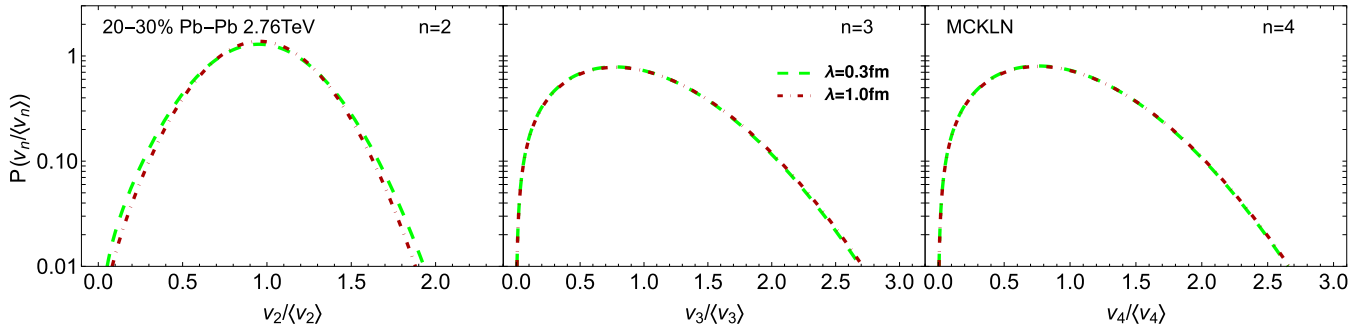

FIG. 7. Comparison of original and filtered scaled v_2 probability distributions for MC-KLN initial conditions.

were computed in Refs. [25,35] (respectively, with URQMD and MC-KLN initial conditions) and exhibit little difference (for coarse-graining size below 1 fm). Harmonic flow $v_n(p_T)$'s were studied in Refs. [25,27,35], small changes were found when the coarse-graining size was varied below 1 fm and other parameters were held fixed. To find observables that depend on the smoothing length, we turn to another quantity, azimuthal correlations. The simplest is a pair correlation:

$$\left\langle \frac{dN_{\text{pairs}}}{d^3p_1 d^3p_2} \right\rangle \propto \left\{ 1 + \sum_{n=1}^{\infty} 2V_{n\Delta}(p_1,p_2)\cos[n(\phi_1-\phi_2)] \right\}. \tag{21}$$

In principle, the Fourier coefficients $V_{n\Delta}(p_1,p_2)$ depend on two momenta, p_1 and p_2, which can be varied independently, and the full matrix has been measured (see, e.g., Ref. [71]).

Since we have already studied the effect of the overall magnitude of anisotropic flow, through momentum integrated measurements, it is convenient to consider a ratio that removes the trivial dependence on ε_n. To that end, we consider the flow factorization ratio [72], which was studied in several works [18,73,74]:

$$r_n(p_1,p_2) = \frac{V_{n\Delta}(p_1,p_2)}{\sqrt{V_{n\Delta}(p_1,p_1)V_{n\Delta}(p_2,p_2)}}. \tag{22}$$

Data for r_n were obtained by CMS [75] and ALICE [76].

This quantity is a good candidate to discriminate smoothing lengths since it was shown in Ref. [73] that r_n could be sensitive to the coarse-graining size but less so to shear viscosity (on this last point see also Refs. [74] and [23] for details on bulk viscosity and hadronic rescattering).

Results for the flow factorization ratios are shown for NeXus and MC-KLN initial conditions in Figs. 9 and 10. Recall that a value $r_n = 1$ is obtained in the absence of p_T-dependent fluctuations. The deviation from unity is therefore a measure of the size of such fluctuations. Thus, we indeed observe a significant dependence on the value of the smoothing scale λ on the size of p_T-dependent fluctuations, and therefore r_n.

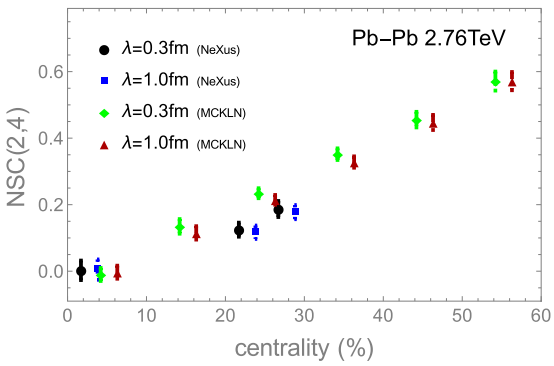

FIG. 8. Comparison of NSC(2,4) for NeXus and MC-KLN original and smoothed initial conditions.

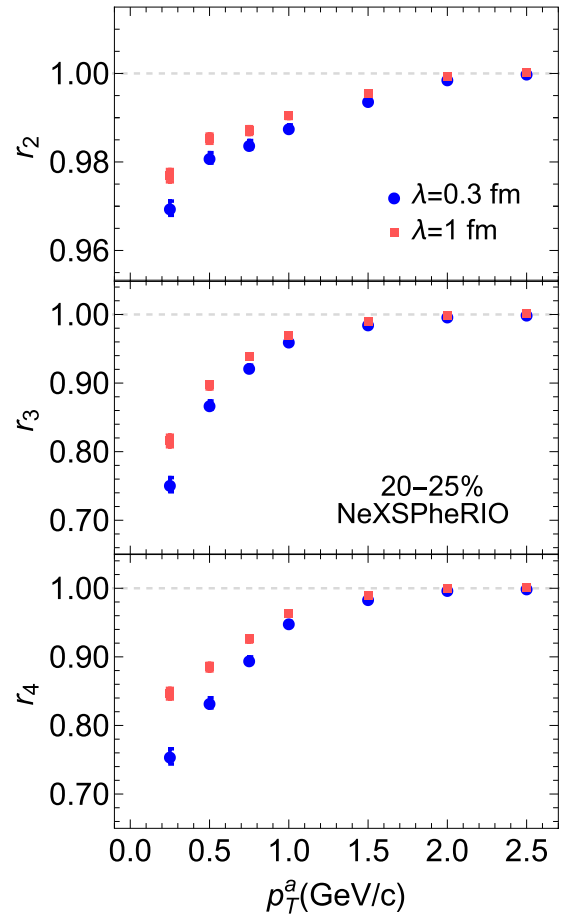

FIG. 9. Flow factorization ratio for NeXus original and smoothed initial conditions in the 20–25% centrality window and 2.5 GeV $< p_T^b <$ 3.0 GeV.

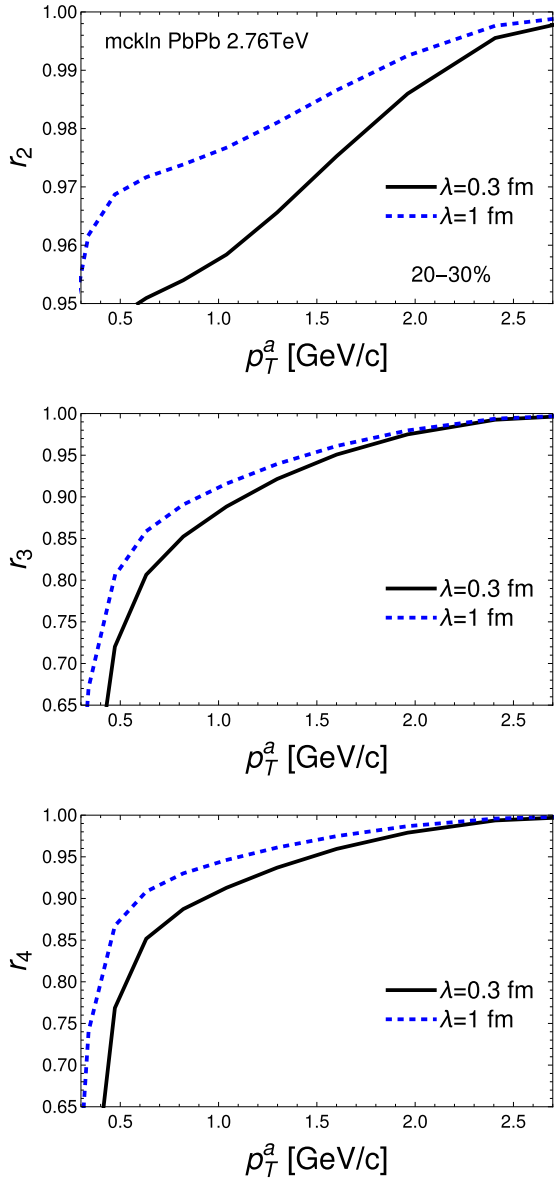

FIG. 10. Flow factorization ratio for MC-KLN original and smoothed initial conditions in the 20–30% centrality window and $p_T^b = 3.0\,\mathrm{GeV}$.

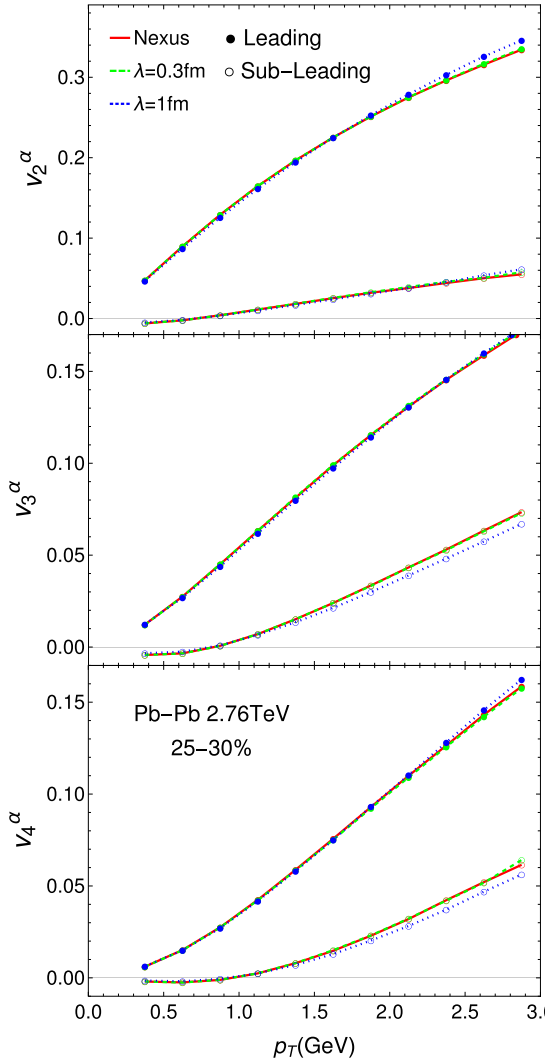

FIG. 11. Leading and subleading components for NeXus original and smoothed initial conditions in the 25–30% centrality class for $n = 2$–4.

In Eq. (22), the trivial decrease of the eccentricity with λ should approximately cancel between numerator and denominator. Therefore, the difference (of order 15% in the most favorable case) is a genuine dependence on smaller scale structures in the initial energy density.

As a final step to search for observables sensitive to coarse-graining size, we perform a principal component analysis (PCA). PCA is a method used in statistics to study data that are possibly correlated. It was suggested to apply it to the matrix formed by the coefficients $V_{n\Delta}(p_1, p_2)$ (with a different normalization than above) in Ref. [69]. A generalization to correlations involving different flow harmonics was proposed in Ref. [77]. Further investigations on the connection with initial geometry were done in Refs. [78,79] and data from CMS have become recently available [80].

We show for $n = 2$–4 the leading principal flow vector (divided by the multiplicity average in the p_T bin) $v_n^{(1)}(p_T)$ in Fig. 11 for the 25–30% centrality bin. The leading components exhibit a small dependence on the smoothing length, consistent with the change in eccentricity. This is expected since they contain similar information to $v_n\{2\}(pT)$ [69], which are not very sensitive to coarse-graining sizes [25,27,35].

We also show for $n = 2$–4 the subleading principal flow vector (again divided by the multiplicity average in the p_T bin) $v_n^{(2)}(p_T)$ in Fig. 11. They exhibit a small dependence on the smoothing length [81]. A dependence is not unexpected since the subleading component is caused by p_T-dependent fluctuations (and has a direct relation to factorization breaking) [69]. While the effect does not appear to be large, it is of measureable size.

V. CONCLUSION

In this paper, to investigate the influence of coarse-graining sizes on observables, we propose a filter to modify the initial

conditions: it smooths the energy density profile in such a way that global properties (as represented by eccentricities ε_n) are kept relatively unchanged, but small-scale structure varies. We consider four models of initial conditions (NeXus, MC-Glauber, MC-KLN, and IP-Glasma) that have very different size of fluctuations. We found that when the smoothing length increases from 0.3 to 1 fm, the eccentricities decrease by n times a few percent, due only to the small increase in system size of the smoothing procedure. Therefore, to find a signal of the coarse-graning sizes in observables scaling with eccentricity, larger changes than that should be seen. In ratio of quantities scaling with eccentricity any dependence may be genuine.

We note that the focus of this paper has been on small-scale structure in large PbPb collisions. Recently, it has been shown that small systems such as pPb and pp may provide more clues about small-scale structure [35,82–85]. We leave a deeper study on small systems for a later work.

We use ideal and viscous hydrodynamics and compute a range of observables. We find that integrated v_n values, scaled v_n distributions, normalized symmetric cumulants, event-plane correlations, leading component in a principal component analysis [and therefore $v_n(p_T)$] do not have a significant dependence on small-scale structure. However the factorization breaking ratio and subleading principle components exhibit nontrivial dependence on the smoothing length. Since the factorization breaking ratio depends little on viscosity, it is the best observable we found to discriminate models that have different fluctuation sizes.

ACKNOWLEDGMENTS

We thank J.-Y. Ollitrault for very helpful discussions on the PCA method. J.N.H. acknowledges the use of the Maxwell Cluster and the advanced support from the Center of Advanced Computing and Data Systems at the University of Houston. F.G. acknowledges support from Fundação de Amparo à Pesquisa do Estado de São Paulo (FAPESP Grants No. 2015/00011-8, No. 2015/50438-8, No. 2016/03274-2), USP-COFECUB (Grant No. Uc Ph 160-16 2015/13), Conselho Nacional de Desenvolvimento Científico e Tecnológico (CNPq Grant No. 310141/2016-8), and project INCT-FNA Proc. No. 464898/2014-5. F.G.G. was supported by Conselho Nacional de Desenvolvimento Científico e Tecnológico (CNPq Grants No. 449694/2014-3 and No. 312203/2015-2) and FAPEMIG (Grant No. APQ-02107-16). F.G.G. and P.M. acknowledge computing time provided on the PdCluster made available by L. F. R. Turci and E. Aguilar (Universidade de Federal de Alfenas/Poços de Caldas). P.I. thanks support from Coordenação de Aperfeiçoamento de Pessoal de Nível Superior (CAPES). M.L. acknowledges support from FAPESP Projects No. 2016/24029-6 and No. 2017/05685-2, and project INCT-FNA Proc. No. 464898/2014-5.

[1] U. Heinz and R. Snellings, Ann. Rev. Nucl. Part. Sci. **63**, 123 (2013).
[2] C. Gale, S. Jeon, and B. Schenke, Int. J. Mod. Phys. A **28**, 1340011 (2013).
[3] R. D. de Souza, T. Koide, and T. Kodama, Prog. Part. Nucl. Phys. **86**, 35 (2016).
[4] S. Jeon and U. Heinz, *Quark gluon plasma 5* (World Scientific Publishing Co., 2016), arXiv:1503.03931.
[5] M. Miller, K. Reygers, S. J. Sanders, and P. Steinberg, Ann. Rev. Nucl. Part. Sci. **57**, 205 (2007).
[6] B. Alver, M. Baker, C. Loizides, and P. Steinberg, arXiv:0805.4411.
[7] C. Loizides, J. Nagle, and P. Steinberg, SoftwareX **1/2**, 13 (2015).
[8] J. S. Moreland, J. E. Bernhard, and S. A. Bass, Phys. Rev. C **92**, 011901 (2015).
[9] H. J. Drescher, M. Hladik, S. Ostapchenko, T. Pierog, and K. Werner, Phys. Rept. **350**, 93 (2001).
[10] T. Pierog, I. Karpenko, J. M. Katzy, E. Yatsenko, and K. Werner, Phys. Rev. C **92**, 034906 (2015).
[11] M. Bleicher *et al.*, J. Phys. G **25**, 1859 (1999).
[12] S. A. Bass *et al.*, Prog. Part. Nucl. Phys. **41**, 255 (1998).
[13] B. Zhang, C. M. Ko, B.-A. Li, and Z.-w. Lin, Phys. Rev. C **61**, 067901 (2000).
[14] H. J. Drescher, F. M. Liu, S. Ostapchenko, T. Pierog, and K. Werner, Phys. Rev. C **65**, 054902 (2002).
[15] H. Niemi, K. J. Eskola, and R. Paatelainen, Phys. Rev. C **93**, 024907 (2016).
[16] H.-J.Drescher and Y. Nara, Phys. Rev. C **75**, 034905 (2007).
[17] B. Schenke, P. Tribedy, and R. Venugopalan, Phys. Rev. Lett. **108**, 252301 (2012).
[18] C. Shen, Z. Qiu, and U. Heinz, Phys. Rev. C **92**, 014901 (2015).
[19] J. E. Bernhard, J. S. Moreland, S. A. Bass, J. Liu, and U. Heinz, Phys. Rev. C **94**, 024907 (2016).
[20] P. Alba, V. M. Sarti, J. Noronha, J. Noronha-Hostler, P. Parotto, I. P. Vazquez, and C. Ratti, arXiv:1711.05207.
[21] G. Giacalone, J. Noronha-Hostler, M. Luzum, and J.-Y. Ollitrault, Phys. Rev. C **97**, 034904 (2018).
[22] K. J. Eskola, H. Niemi, R. Paatelainen, and K. Tuominen, Phys. Rev. C **97**, 034911 (2018).
[23] S. McDonald, C. Shen, F. Fillion-Gourdeau, S. Jeon, and C. Gale, Phys. Rev. C **95**, 064913 (2017).
[24] T. Renk and H. Niemi, Phys. Rev. C **89**, 064907 (2014).
[25] H. Petersen, C. Coleman-Smith, S. A. Bass, and R. Wolpert, J. Phys. G **38**, 045102 (2011).
[26] C. E. Coleman-Smith, H. Petersen, and R. L. Wolpert, J. Phys. G **40**, 095103 (2013).
[27] Md. R. Haque, V. Roy, and A. K. Chaudhuri, Phys. Rev. C **86**, 037901 (2012).
[28] A. Bzdak, B. Schenke, P. Tribedy, and R. Venugopalan, Phys. Rev. C **87**, 064906 (2013).
[29] S. Floerchinger and U. A. Wiedemann, Phys. Lett. B **728**, 407 (2014).
[30] S. Floerchinger and U. A. Wiedemann, Phys. Rev. C **88**, 044906 (2013).
[31] S. Floerchinger and U. A. Wiedemann, Phys. Rev. C **89**, 034914 (2014).
[32] E. Retinskaya, M. Luzum, and J.-Y. Ollitrault, Phys. Rev. C **89**, 014902 (2014).
[33] V. P. Konchakovski, W. Cassing, and V. D. Toneev, J. Phys. G **42**, 055106 (2015).

[34] R. S. Bhalerao, M. Luzum, and J.-Y. Ollitrault, Phys. Rev. C **84**, 054901 (2011).
[35] J. Noronha-Hostler, J. Noronha, and M. Gyulassy, Phys. Rev. C **93**, 024909 (2016).
[36] L. Keegan, A. Kurkela, A. Mazeliauskas, and D. Teaney, J. High Energy Phys. 08 (2016) 171.
[37] D.Teaney and L.Yan, Phys. Rev. C **83**, 064904 (2011).
[38] H. Niemi, G. S. Denicol, H. Holopainen, and P. Huovinen, Phys. Rev. C **87**, 054901 (2013).
[39] J. Fu, Phys. Rev. C **92**, 024904 (2015).
[40] J. Noronha-Hostler, B. Betz, J. Noronha, and M. Gyulassy, Phys. Rev. Lett. **116**, 252301 (2016).
[41] J. Noronha-Hostler, B. Betz, M. Gyulassy, M. Luzum, J. Noronha, I. Portillo, and C. Ratti, Phys. Rev. C **95**, 044901 (2017).
[42] C. A. G. Prado, J. Noronha-Hostler, R. Katz, A. A. P. Suaide, J. Noronha, and M. G. Munhoz, Phys. Rev. C **96**, 064903 (2017).
[43] C. Aguiar, T. Kodama, T. Osada, and Y. Hama, J. Phys. G **27**, 75 (2001).
[44] Y. Hama, R. P. Andrade, F. Grassi, O. S. Jr., T. Kodama, B. Tavares, and S. S. Padula, Nucl. Phys. A **169**, 774 (2006).
[45] W. L. Qian, R. Andrade, F. Grassi, J. O. Socolowski, T. Kodama, and Y. Hama, Int. J. Mod. Phys. E **16**, 1877 (2007).
[46] R. P. G. Andrade, F. Grassi, Y. Hama, T. Kodama, and J. O. Socolowski, Phys. Rev. Lett. **97**, 202302 (2006).
[47] R. P. G. Andrade, F. Grassi, Y. Hama, T. Kodama, and W. L. Qian, Phys. Rev. Lett. **101**, 112301 (2008).
[48] R. P. G. Andrade, A. dos Reis, F. Grassi, Y. Hama, W. Qian, T. Kodama, and J.-Y. Ollitrault, Acta Phys. Polon. B **40**, 993 (2009).
[49] F. G. Gardim, F. Grassi, Y. Hama, M. Luzum, and J. Y. Ollitrault, Phys. Rev. C **83**, 064901 (2011).
[50] F. G. Gardim, F. Grassi, M. Luzum, and J.-Y. Ollitrault, Phys. Rev. Lett. **109**, 202302 (2012).
[51] J. Takahashi, B. M. Tavares, W. L. Qian, R. Andrade, F. Grassi, Y. Hama, T. Kodama, and N. Xu, Phys. Rev. Lett. **103**, 242301 (2009).
[52] W.L.Qian, R. P. G. Andrade, F. Gardim, F. Grassi, and Y. Hama, Phys. Rev. C **87**, 014904 (2013).
[53] M. V. Machado, Event-by-event Hydrodynamics for the LHC, Master's thesis, Universidade de São Paulo, Brazil, 2015.
[54] J. Noronha-Hostler, G. S. Denicol, J. Noronha, R. P. G. Andrade, and F. Grassi, Phys. Rev. C **88**, 044916 (2013).
[55] J. Noronha-Hostler, J. Noronha, and F. Grassi, Phys. Rev. C **90**, 034907 (2014).
[56] P. Huovinen and P. Petreczky, Nucl. Phys. A **837**, 26 (2010).
[57] TECHQM, https://wiki.bnl.gov/TECHQM/index.php/Code_checking_list.
[58] H. Marrochio, J. Noronha, G. S. Denicol, M. Luzum, S. Jeon, and C. Gale, Phys. Rev. C **91**, 014903 (2015).
[59] J. Jia (ATLAS collaboration), Nucl. Phys. A **904-905**, 421c (2013).
[60] G. Aad *et al.* (ATLAS collaboration), J. High Energy Phys. 11 (2013) 183.
[61] A. R. Timmins (ALICE collaboration), J. Phys. Conf. Ser. **446**, 012031 (2013).
[62] C. Gale, S. Jeon, B. Schenke, P. Tribedy, and R. Venugopalan, Phys. Rev. Lett. **110**, 012302 (2013).
[63] W. Zhao, H.-j. Xu, and H. Song, Eur. Phys. J. C **77**, 645 (2017).
[64] L. Barbosa, F. Gardim, F. Grassi, P. Ishida, M. Luzum, and M. V. Machado (unpublished).
[65] J. Noronha-Hostler, L. Yan, F. G. Gardim, and J.-Y. Ollitrault, Phys. Rev. C **93**, 014909 (2016).
[66] Y. Zhou *et al.* (ALICE collaboration), Nucl. Phys. A **956**, 296 (2016).
[67] J. Adam *et al.* (ALICE collaboration), Phys. Rev. Lett. **117**, 182301 (2016).
[68] F. G. Gardim, F. Grassi, M. Luzum, and J. Noronha-Hostler, Phys. Rev. C **95**, 034901 (2017).
[69] R. S. Bhalerao, J.-Y. Ollitrault, S. Pal, and D. Teaney, Phys. Rev. Lett. **114**, 152301 (2015).
[70] G. Aad *et al.* (ATLAS collaboration), Phys. Rev. C **90**, 024905 (2014).
[71] K. Aamodt *et al.* (ALICE collaboration), Phys. Lett. B **708**, 249 (2012).
[72] F. G. Gardim, F. Grassi, M. Luzum, and J.-Y. Ollitrault, Phys. Rev. C **87**, 031901(R) (2012).
[73] I. Kozlov, M. Luzum, G. Denicol, S. Jeon, and C. Gale, arXiv:1405.3976.
[74] U. Heinz, Z. Qiu, and C. Shen, Phys. Rev. C **87**, 034913 (2013).
[75] V. Khachatryan *et al.* (CMS), Phys. Rev. C **92**, 034911 (2015).
[76] S. Acharya *et al.* (ALICE), J. High Energy Phys. 09 (2017) 032.
[77] P. Bożek, Phys. Rev. C **97**, 034905 (2018).
[78] A. Mazeliauskas and D. Teaney, Phys. Rev. C **91**, 044902 (2015).
[79] A. Mazeliauskas and D. Teaney, Phys. Rev. C **93**, 024913 (2016).
[80] A. M. Sirunyan *et al.* (CMS), Phys. Rev. C **96**, 064902 (2017).
[81] We leave a detailed comparison of CMS data with 3+1 hydro to a future work.
[82] K. Welsh, J. Singer, and U. W. Heinz, Phys. Rev. C **94**, 024919 (2016).
[83] J. L. Albacete, H. Petersen, and A. Soto-Ontoso, Phys. Lett. B **778**, 128 (2018).
[84] G. Giacalone, J. Noronha-Hostler, and J.-Y. Ollitrault, Phys. Rev. C **95**, 054910 (2017).
[85] J. S. Moreland, J. E. Bernhard, W. Ke, and S. A. Bass, in *Proceedings of the 26th International Conference on Ultrarelativistic Nucleus-Nucleus Collisions (Quark Matter 2017)*, Nucl. Phys. A **967**, 361 (2017).